Chapter 7
Application of Footprint Models to Different Measurement Techniques

Footprint models were mainly developed to interpret the results of flux measurement techniques. The aim was to replace the *ad hoc* typical 'empirical rule' used in the past to determine optimal measurement conditions. According to this rule, the ratio of the measuring height to that of the undisturbed fetch on the upwind site is of approximately 1:100. Since such simple assumptions were reasonable in pre-footprint time (before 1990), most micrometeorological experiments took place over homogeneous surfaces, typically using short towers over agricultural crops. In those days, the eddy-covariance technique was not used in ecology and in environmental fields. As the eddy-covariance flux method grew in popularity, more sophisticated approaches with realistic assumptions—a footprint analysis—had to be developed and applied along with the need for a theoretical framework explaining its physical underpinnings. The different flux measurement methods are divided into direct ones for which flux footprint models were developed or indirect methods for which mainly footprint models for scalars are relevant. In the following chapter, these measurement techniques are discussed in relation to the use of footprint models.

7.1 Profile Technique

The profile method is based on flux-gradient similarity (see Sect. 2.2.1). It is an indirect method, because the turbulent Prandtl number and universal functions must be determined in comparison with a direct method, such as the eddy-covariance

M. Y. Leclerc and T. Foken, *Footprints in Micrometeorology and Ecology*,
DOI: 10.1007/978-3-642-54545-0_7, © Springer-Verlag Berlin Heidelberg 2014

technique (see Sect. 7.2). Because of the advantages of the eddy-covariance method in the last 15 years, the profile method is seldom often used. Many considerations including internal boundary layers in the footprint area and measurements over heterogeneous surfaces are limitations that have hindered the dissemination and application of this method. More often, simplified methods with only two measuring heights are used mainly in applied meteorology (Agrometeorology etc.). But all approaches are significantly influenced by the footprint because measurements are made in different heights but each sensor must be influenced by the same underlying surface type for all wind velocities and stability conditions.

7.1.1 *Profile Technique with Three and More Measuring Levels*

The profile method uses approximately 4–6 levels with wind, temperature, humidity or trace gas measurements (Fig. 7.1). The basis for the method lies in the neutral case Eqs. (2.16–2.18). From the measured profile, it is necessary to determine the gradient of the state parameters. In the simplest case, this can be done using a linear approximation, a method also used in approaches with only two measuring heights. Therefore a diagram is necessary with the wind velocity u—can by replaced by the temperature or trace gas concentration—on the abscissa and z on the ordinate, were the differential $\partial u/\partial z$ can determined by the differences of both, u and z (Fig. 7.2a).

$$\left(\frac{\partial u}{\partial z}\right)_{z_a} \cong \frac{\Delta u}{\Delta z} = \frac{u_2 - u_1}{z_2 - z_1} \qquad z_a = (z_2 - z_1)/2 \tag{7.1}$$

A much better application of the physical background is a logarithmical approximation with a geometric average of the measurement heights. In this approach, a diagram with u, T, or c on the abscissa and z on the vertical ordinate is which has a logarithmical scale (Fig. 7.2b):

$$\left(\frac{\partial u}{\partial \ln z}\right)_{z_m} \cong \frac{\Delta u}{\Delta \ln z} = \frac{u_2 - u_1}{\ln(z_2/z_1)} \qquad z_m = (z_1 \cdot z_2)^{1/2} \tag{7.2}$$

The basis for the profile method in the non-neutral case can be found in Eqs. (2.24)–(2.26). The simplest way is to use the integrated form of Eq. (2.28) and compares on the ordinate ($\ln z - \psi(z/L)$) and in case of the wind profile on the abscissa u (Fig. 7.2c). The following equation can be used for the momentum and the sensible heat fluxes as an example (Arya 2001):

Fig. 7.1 Measuring tower for profile measurements, *Photograph* Foken

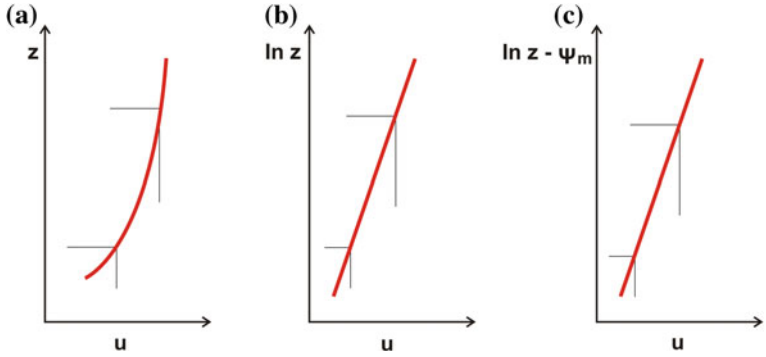

Fig. 7.2 Approximations of the profile function **a** with a linear approximation with Eq. (7.1), **b** with a lin-log approximation for the neutral case with Eq. (7.2), **c** with the lin-log approximation for the non-neutral case with Eq. (7.3). The red line is the measured profile and the thin lines are the range for determination the differences for the gradient

$$\ln z - \psi_m(z/L) = \frac{\kappa}{u_*} \cdot u + \ln\, z_0 \tag{7.3}$$

$$\ln z - \psi_H(z/L) = \frac{\kappa}{\mathrm{Pr}_t\, T_*} \cdot T - \frac{\kappa}{\mathrm{Pr}_t\, T_*} \cdot T_0 + \ln\, z_0 \tag{7.4}$$

The Obukhov length or the Richardson number (see Sect. 2.2.1) is necessary for this approximation. It can be determined by an iterative solution of Eqs. (7.3) and (7.4). Several approaches can be used for the interpolation of the profile function

such as the cubic spline method. Because of possible measurements errors, an overshoot can influence the results. Therefore, the choice of the approximation function should be carefully done, e.g. the spline method by Akima (1970) has often been successfully used.

Often applied is the Nieuwstadt-Marquardt-approach. Therefore, the quadratic cost function as a measure of the differences between measuring values and the profile equation are calculated (Nieuwstadt 1978). The non-linear system of equations of the minimization of the deviations can be solved using the method by Marquardt (1983).

7.1.2 Profile Technique with Two Measuring Levels

The Bowen-ratio method (Bowen 1926) is the most popular approach to determine sensible and latent heat fluxes mainly in agricultural meteorology. The method is based on the Bowen-ratio and the energy balance equation (Fritschen and Fritschen 2005; Foken 2008):

$$Bo = \frac{Q_H}{Q_E} \approx \gamma \cdot \frac{\Delta T}{\Delta e} \tag{7.5}$$

$$-Q_s^* = Q_H + Q_E + Q_G \tag{7.6}$$

The psychrometric constant is $\gamma = 0.667$ K hPa^{-1} for p = 1013 hPa and t = 20 °C. From both Equations follows for the sensible and latent heat flux:

$$Q_H = \left(-Q_s^* - Q_G\right) \frac{Bo}{1 + Bo} \tag{7.7}$$

$$Q_E = \frac{-Q_s^* - Q_G}{1 + Bo} \tag{7.8}$$

The experimental setup consists of measurements at two levels for temperature and humidity and additionally a net radiometer and a soil heat flux plate and soil temperature sensor (Fig. 7.3). The approximation in Eqs. (7.5) to (7.8) depends on several assumptions, which are discussed in more details, e.g. by Ohmura (1982) or Foken (2008). It is essential that the turbulent atmospheric conditions be fulfilled for wind velocities in the upper measurement level of >1 m s^{-1} and/or a difference of the wind velocity between both levels of >0.3 m s^{-1} are necessary. Furthermore, the ratio of both measuring heights should be 4–8 to ensure that the temperature, humidity etc. difference between both levels is significantly larger than the measurement error.

A special version of the Bowen-ratio method is the Modified Bowen-ratio method, which was developed mainly for trace gas fluxes (Businger 1986) and can also be applied for energy fluxes (Liu and Foken 2001). Such a system is shown in

Fig. 7.3 Bowen-ratio system (*Photograph* Campbell Scientific Inc. Logan UT, USA, Published with kind permission of © Campbell Sci. Inc., 2012. All Rights Reserved)

Fig. 7.4. Equation (7.5) and the measurements set up at two levels are analogous to the standard Bowen-ratio method. Only one flux, often the sensible heat flux, is directly measured with the eddy-covariance method (see Sect. 7.2). From the definition of the Bowen-ratio, the latent heat flux can easily be determined. In the case of trace gas fluxes, the measurement of the humidity gradient is replaced by the gradient of the trace gas and the modified Bowen-ratio is defined as the ratio of the sensible to the trace gas flux. Since a sonic anemometer measures the buoyancy flux (see Sect. 7.2), this flux must be transformed into the sensible heat flux (Schotanus et al. 1983; Foken et al. 2012a) or the temperature gradient must be replaced by the gradient of the virtual temperature. With the sonic anemometer, the wind velocity can be controlled and no additional anemometer is necessary.

Additional methods to parameterize the fluxes with measurements at two levels are given by Foken (2008).

Fig. 7.4 Modified Bowen-ratio system for sensible and latent heat flux according to Liu et al. (2001), *Photograph* by Foken

7.1.3 Accuracy and Footprint Issues for Profile Technique

The basis for this method is (1) the assumption that the differences of the measurement signal between two adjacent measuring levels is significant larger than the measurement error of the sensor and (2) the assumption is that the influence of the vertical exchange process on the differences is significant larger than possible effects of different footprint areas on the measured signal on the different measurement levels. Because the last assumption cannot easily be fulfilled, surface characteristics in footprint areas of the different measuring levels should be equal to one another. The consequence may be that, for limited fetch conditions, the range of the measurement height decreases with an increase in stability. Furthermore, no internal boundary layers should influence the profile measurements (see Sect. 8.1). In the case when the differences in the footprint between the levels of the profile method cause differences in the temperature, moisture, and trace gas measurements which are larger as the minimal errors of the system, the error due to the different footprints determine the error of the whole system.

Table 7.1 Minimal measurable flux (20 % error) for energy and trace gases above low, $z_2/z_1 = 8$, and tall, $z_2/z_1 = 1.25$, vegetation for neutral stratification and $u_* = 0.2$ m s^{-1} (dimensions µg m^{-3} and µg s^{-1} m^{-2}), the "*italic*" fluxes are lager as the typical fluxes in the nature (Foken 1998, 2008)

Energy and matter flux	χ_{min}	$\Delta_{\chi,min}$	Flux $z_2/z_1 = 8$	Flux $z_2/z_1 = 1.25$
Sensible heat	0.05 K	0.5 K	0.025 m K s^{-1} 30 W m^{-2}	0.05 m K s^{-1} 60 W m^{-2}
Latent heat	0.05 hPa	0.5 hPa	0.025 hPa K s^{-1} 45 W m^{-2}	0.05 hPa K s^{-1} 90 W m^{-2}
Nitrate particles	0.01	0.1	0.005	0.01
Ammonium particles	0.02	0.2	0.01	*0.02*
CO_2	100	1000	50	100
NO	0.06	0.6	*0.03*	*0.06*
NO_2	0.1	1.0	0.05	0.1
O_3	1.0	10.0	0.5	*1.0*
NH_3	0.014	0.14	0.007	0.014
HNO_3	0.2	2.0	*0.1*	*0.2*
HNO_2	0.25	2.5	*0.125*	*0.25*

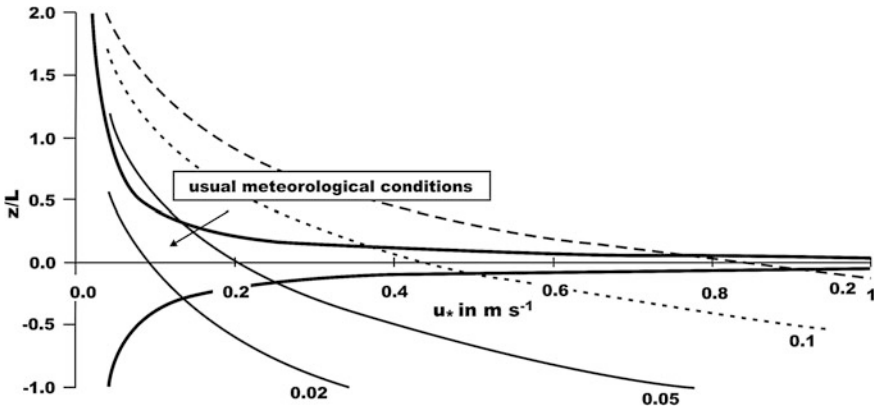

Fig. 7.5 The normalized flux Q_N (numbers are written in the *hyperbolic lines*) depending on stratification and the friction velocity for $z_2/z_1 = 8$ (Foken 2008). The typical range of meteorological measurements is between the *black lines*

7.1.3.1 Accuracy of Profile Measurements

The first assumption can be more easily controlled. According to Foken (1998, 2008), the profile Eqs. (2.16)–(2.18) can be divided into a term depending on the dynamical-thermal turbulence Q_N and another term, namely, the difference of the state parameter between the different measurement levels $\Delta\chi$.

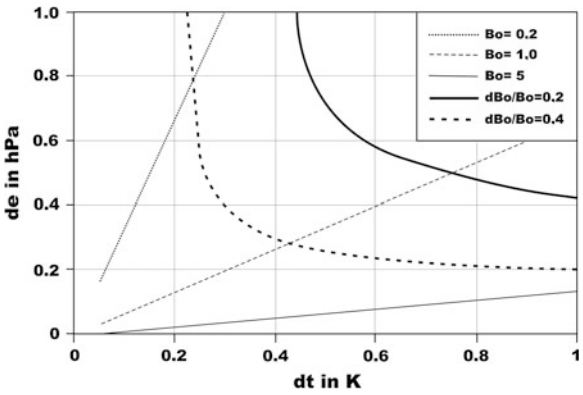

Fig. 7.6 Error of the Bowen-ratio (20 and 40%) determined with the Bowen-ratio method dependent on the temperature and moisture difference in between both levels (Foken et al. 1997). The accuracy of the measuring system is ± 0.05 K and hPa, Published with kind permission of © Zentralanstalt für Meteorologie und Geodynamik, 1997. All Rights Reserved

$$Q_\chi = Q_N[u_*, \varphi(z/L), \ln(z-d)] \cdot \Delta\chi \tag{7.9}$$

The normalized flux Q_N is shown in Fig. 7.5. The minimal fluxes, which can be measured with an accuracy of 20 %, depend on the tenfold accuracy of the measurement system χ_{min}:

$$Q_{\chi,\min} = Q_N \cdot 10 \cdot \chi_{\min} \tag{7.10}$$

Typical values of measurable fluxes above low and tall vegetation are given in Table 7.1. This table can be used in the following way: Only typical values of the accuracy of the measurement system are given in the Table. With the specification of the system, one can use Eq. (7.10) and find the minimal flux which can be measured with an accuracy of 20 %. Therefore, one has to determine the Q_N value according to meteorological conditions (stratification, friction velocity) from Fig. 7.5. The figure is calculated for a ratio $z_2/z_1 = 8$, which applies only above low vegetation. Going back to Table 7.1, one can see the difference to high vegetation $z_2/z_1 = 1.25$. So this is a simple approach to check for which fluxes which accuracy of the measurements is necessary to make flux measurements with the two levels profile approach. If the number of levels goes up, one can increase also the accuracy and can easily determine whether measurements at one level represent the surface of interest or not. Not included in this system is the influence of the roughness sub layer, which must be taken into account above tall vegetation. Due to a higher mixing above a forest canopy for instance, the gradient is even more reduced, up to a factor of 2 (enhancement factor) and therefore the accuracy of the system must be assumed to be twice as high as what is stated in the Table 7.1 to determine the accuracy of the final flux.

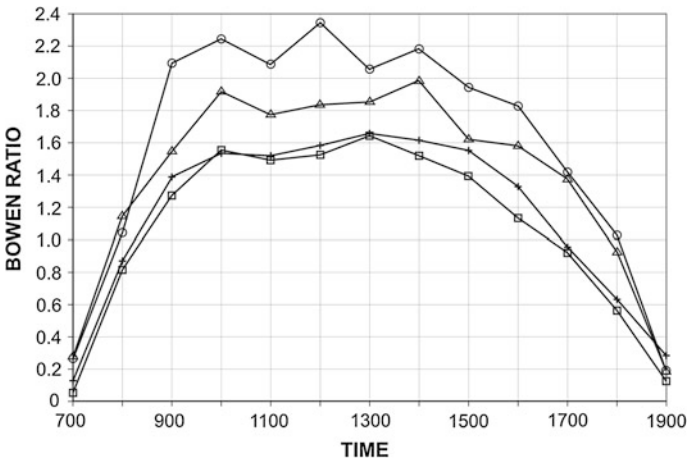

Fig. 7.7 Bowen-ratio measurements by Tanner (1988) with two systems (+, □) at one day in the same level and at a second day in two different levels (△, ◇) (Leclerc and Thurtell 1990, figure was reconstructed)

In the case of a Bowen-ratio system, a simpler approach was given by Foken et al. (1997). Assuming an error in the measurement set up of ± 0.05 K or hPa for temperature and moisture measurements, Fig. 7.6 shows the ranges with a possible error in the Bowen-ratio. Note that the error of the temperature and moisture measurements in the atmosphere is significantly higher than the pure instrumentation error (Dugas et al. 1991). An error in the Bowen ratio of 0.1 is related to a flux error of 10 %. For this case, typical differences between both measurement levels should not only be in the order of 0.5 K and 0.5 hPa but also in a range of the Bowen ratio of about 0.3–1.0. Therefore, the method fails in the case of very dry or humid conditions.

7.1.3.2 Footprint of Profile Measurements

A first example of the influence of the footprint on the Bowen-ratio in the field was discussed in Leclerc and Thurtell (1990) and was the link to develop their Lagrangian simulation (see Sect. 3.2.1). Two systems on the same point and in the same height showed identical Bowen-ratios, but the application of these two systems in different heights showed because of the different footprint of both systems, which included for the upper system a second field with different land use, significant different values (Fig. 7.7).

An illustration of the footprint problem was also given by Schmid (1997). That study shows that in Fig. 7.8 three measuring heights have a different footprint area and covers different types of surfaces. In such a case, the profile approach would not measure only vertical gradients but also horizontal differences of different land cover. Therefore, the profile tower should be placed left of the cross in Fig. 7.8, at

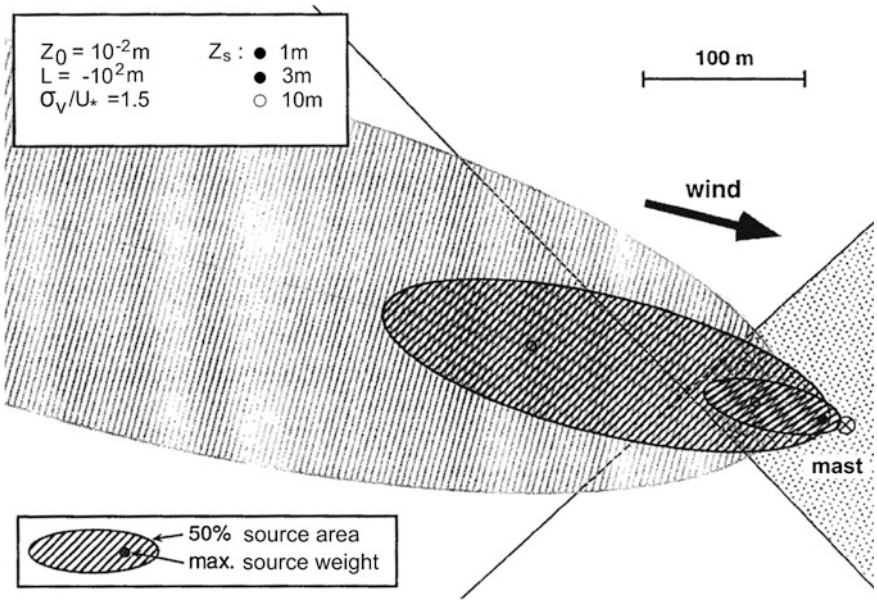

Fig. 7.8 Footprint area for different measuring heights covering different surfaces (Schmid 1997, Published with kind permission of © Elsevier, 1997. All Rights Reserved)

the junction of the four different surface types. Short of using this method, it is likely that the experimentalist will be unable to interpret the data. Sometimes the differences of the underlying surfaces may not be small so that a profile approach appears impossible. The footprint area of all sensors must be identical in size and must complete cover only one surface type. The data can be tested by the representativity test (Nappo et al. 1982).

Horst (1999) pointed out that the simple concentration footprint related approach by Schmid (1997) does not perform the conditions of the profile technique because the gradient approach has a special flux footprint: Based on a previous study by Stannard (1997), Horst (1999) extended his model (Horst and Weil 1992, 1994) to estimate footprint fluxes obtained from micrometeorological profile techniques. He presented a formulation for use with the concentration profile to estimate flux footprints and for fluxes measured using the Bowen-ratio technique.

While a flux footprint can be theoretically derived for concentration measurements made at two or more levels as is the case in Bowen-ratio and profile methods, the reader is therefore reminded that this method, in practice, works only in the special case where tower concentration sensors see a consistency in the emission rate of the surface within their different footprints. The flux footprint for the Bowen-ratio technique is identical to that for a two-level profile measurement only for very limited circumstances. In the more general case, a flux footprint cannot be defined when using the Bowen-ratio technique.

The full derivation is found in Horst (1999), with the resulting flux footprint equation determined from measurements made at two levels as in the Bowen ratio method, can be expressed as

$$\overline{f}^{y} = -\frac{\mathrm{A\,u_{*}}\kappa}{\overline{\mathrm{z}}\mathrm{U}} \frac{\exp^{-(\mathrm{z_2}/\mathrm{b}\overline{\mathrm{z}})^{\mathrm{r}}} - \exp^{-(\mathrm{z_1}/\mathrm{b}\overline{\mathrm{z}})^{\mathrm{r}}}}{\ln\left(\mathrm{z_2}/\mathrm{z_1}\right) - \psi\left(\mathrm{z_2}/\mathrm{L}\right) + \psi\left(\mathrm{z_1}/L\right)} \tag{7.11}$$

In the case of the concentration-profile footprint flux estimates, Horst (1999) found the upwind extent of the footprint for concentration-profile flux estimates to be similar to that of the footprint for eddy-covariance flux measurements when the eddy-covariance measurement is made at a height equal to the arithmetic mean of the highest and lowest profile measurement height for stable stratification or the geometric mean for unstable stratification. The resulting expression for a flux footprint determined from a multiple level concentration measurement is

$$\overline{f}^{y} = -\frac{Au_{*}\kappa}{\overline{z}u\varphi_{m}\left(z_m/L\right)} \sum_{j=1}^{n} b_j e^{-(z_j/b\overline{z})^{r}} \tag{7.12}$$

According to the theoretical approach by Horst (1999), the concentration-profile flux footprint depends on the ratio of the highest to the lowest measurement height, but appears to be insensitive to the number of measurement levels. That study also found that the concentration-profile flux footprint extends closer to the measurement location than does the 'equivalent' eddy-covariance flux footprint, with the difference becoming more pronounced as the ratio of the profile measurement heights increases. For the Modified Bowen-ratio system, it can then be concluded that the limiting factor in the footprint is the flux measurements with the sonic anemometer, because the anemometer is installed above the profile measuring levels.

7.2 Eddy–Covariance Technique

7.2.1 Basics of the Eddy-Covariance Method

The eddy covariance method based on the transfer equations for momentum, heat, humidity or trace gases by application of the Reynolds's decomposition (Businger 1982; Stull 1988; Foken 2008; Foken et al. 2012b), which divides a turbulent parameter x into a mean part $\overline{x}$ and into a fluctuating part x' (Fig. 7.9)

$$\mathrm{x} = \overline{\mathrm{x}} + x'. \tag{7.13}$$

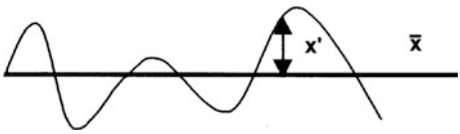

Fig. 7.9 Schematic presentation of Reynolds's decomposition of the value x (Foken 2008)

By neglecting the pressure gradient, molecular/viscous transport, gravity and Coriolis terms which have no significant impact on the eddy-covariance method over flat terrain the equation can be simplified. The coordinate system must be chosen in such a way that the perpendicular, $\overline{v}$, and vertical, $\overline{w}$, wind component are zero and assuming horizontal homogeneity as well as steady-state conditions. For the momentum flux follows finally:

$$\frac{\partial \overline{w'u'}}{\partial z} = 0 \tag{7.14}$$

where $\overline{u'w'}$ is the eddy covariance term for the momentum flux. The eddy-covariance terms are analogous to the former, as for the sensible heat flux $\overline{w'T'}$, for the latent heat flux $\overline{w'q'}$, and $\overline{w'\chi'}$ for the trace gas flux. From Eq. (7.14) follows that, under the preceding assumptions, this flux is constant with height and that it is representative of the vertical flux through a horizontal plane above the surface roughness elements. This approach is called the eddy-covariance method. More details and necessary assumptions are given in the relevant literature (Lee et al. 2004; Foken 2008; Aubinet et al. 2012), but most important are the assumption on steady-state conditions and horizontal homogeneous surfaces. Furthermore, the mean vertical wind velocity must equal zero for the equation of the total flux to hold (Reynolds' postulate; Eq. 2.5), i.e.

$$\overline{wx} = \bar{w}\bar{x} + \overline{w'x'} \tag{7.15}$$

Therefore, the flux can only be determined with the covariance term provided this assumption is fulfilled. The assumption will be fulfilled by an coordinate transformation where recently the planar-fit method is recommended (Wilczak et al. 2001). This method is applied for longer periods like weeks or months to avoid strong influences of single burst and gusts.

According to Eq. (7.15) the turbulent fluctuations of the components of the wind vector and of scalar parameters must be measured at a high sampling frequency so that the turbulence spectra can be extended to 10–20 Hz. The measuring devices used for such purposes are sonic anemometers for the wind components and sensors that can measure scalars with the required high resolution in time. The latter are often optical measurement methods. The sampling time depends on atmospheric stability, wind velocity, and measuring height. Such a measurement complex is shown in Fig. 7.10. According to the theory, the method is a direct one without any empirical function. Nevertheless, the simplifications given above and instrumental problems need a set of corrections. Literature is available regarding

Fig. 7.10 Measuring complex for eddy-covariance measurements consistent on a sonic anemometer CSAT3 and an IR gas analyser LiCor 7500 (*Photograph* by Foken)

these issues (Haugen 1973; Kaimal and Finnigan 1994; Lee et al. 2004; Foken 2008; Aubinet et al. 2012).

Because the eddy-covariance technique is often not applied in homogeneous terrain, the influence of different underlying surface conditions must be taken into account in the data interpretation. This was the main reason behind the development of footprint techniques.

7.2.2 1D Eddy-Covariance Method

Eddy-covariance measurements can be used to estimate fluxes of energy, heat, water vapor, and gases between the ecosystem and the atmosphere. The method was described above in such a way that the measurement above the canopy represents the flux between the atmosphere and the ecosystem (Fig. 7.11). This 1D net ecosystem flux is the sum of the eddy-covariance measurements (term II) and the change of the storage (term I). Term V is a sink or source term.

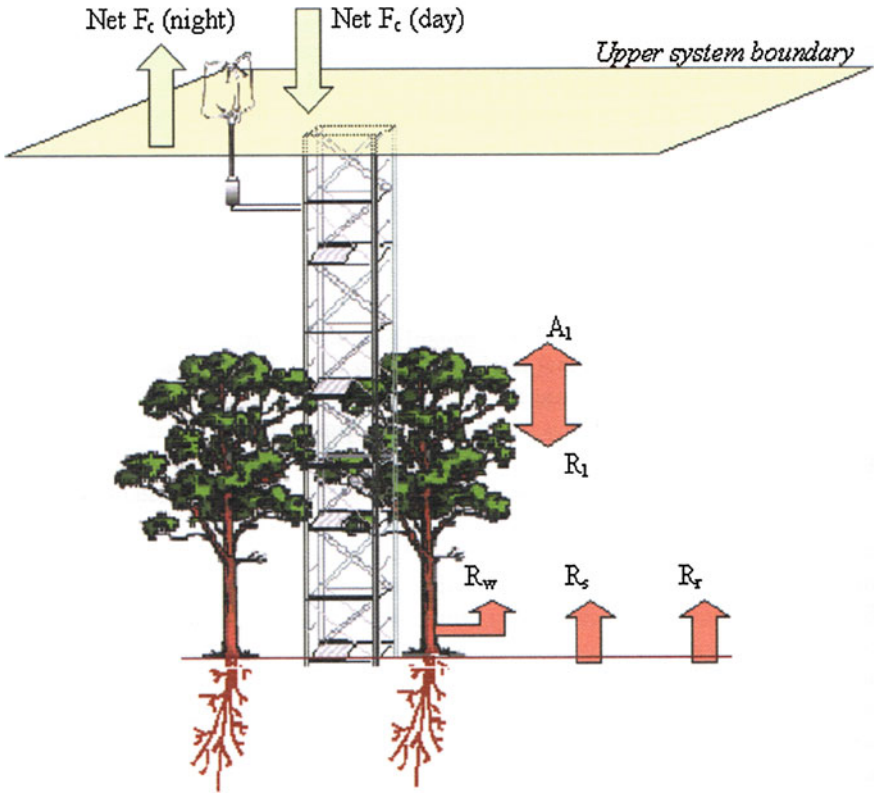

Fig. 7.11 Determination of the net ecosystem exchange with the eddy-covariance method with the assumption of a point measurement (Moncrieff 2004) with A: assimilation and R: different respiration pathways

$$\underbrace{\int_0^{z_m} \overline{\rho_d} \frac{\overline{\partial \chi}}{\partial t}}_{I} + \underbrace{\overline{\rho_d} \overline{w' \chi'}|_h}_{II} = \underbrace{\overline{\sum}}_{V} \tag{7.16}$$

For this assumption all flux footprint models including all analytical models can be applied.

7.2.3 Generalized Eddy-Covariance Method (3D)

In reality, the ecosystem is more complex and an equation for a volume element must be formulated (Fig. 7.12). The expression for the ecosystem exchange is

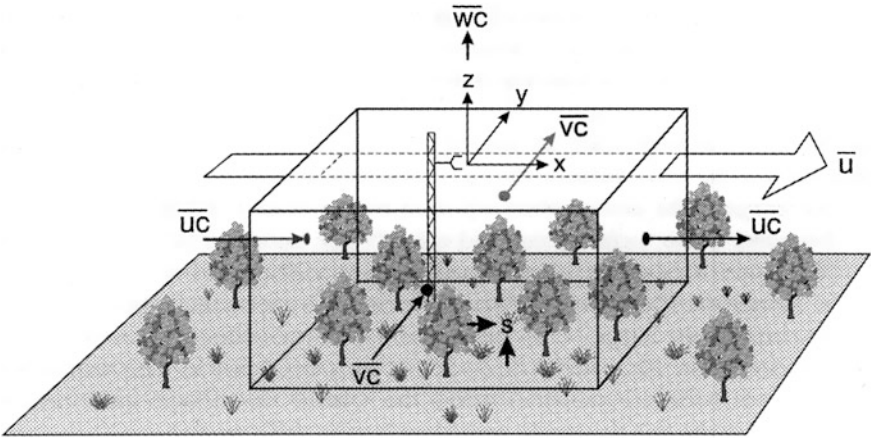

Fig. 7.12 Schematic image of integration of Eq. (7.17) on a control volume in homogeneous terrain (Finnigan et al. 2003)

$$\underbrace{\int_0^{z_m} \overline{\rho_d}\,\frac{\overline{\partial \chi}}{\partial t}\,dz}_{I} + \underbrace{\overline{\rho_d}\,\overline{w'\chi'}\big|_{z_m}}_{II} + \underbrace{\int_0^{z_m}\left[\overline{\rho_d u}\,\frac{\Delta\overline{\chi}_x}{\Delta x} + \overline{\rho_d v}\,\frac{\Delta\overline{\chi}_y}{\Delta y}\right]}_{III} + \underbrace{\int_0^{z_m}\left[\overline{\rho_d w}\,\frac{\Delta\overline{\chi}}{\Delta z}\right]}_{IV} = \underbrace{\overline{\sum}}_{V} \tag{7.17}$$

This includes besides the terms I and II also the horizontal advection (term III) and the vertical advection (term IV). The often neglected convergence or divergence of the horizontal flux is not included in Eq. (7.17). This flux may be averaged over time and integrated both horizontally over the area and vertically, from the ground to instrument height z_m (Fig. 7.12). This approach is now called the "generalized eddy-covariance" method (Foken et al. 2012b). Simple analytic footprint models cannot handle this volume average but for Lagrangian models with in-canopy turbulence parameterization, this is partly possible (Baldocchi 1997; Rannik et al. 2000, 2003; Lee 2004).

It is extremely difficult and cost intensive to measure the terms III and IV: recent and carefully planned special advection experiments fell short of expectations (Aubinet 2008). Often the terms III and IV are of the same order with the different sign and the influence on the net ecosystem exchange is negligible. Nevertheless, possible effects of the advection should be tested for a specific site at least with a special designed short-term experiment. Because of these problems, the generalized eddy-covariance technique is often reduced to the 1D version.

Table 7.2 Possible combination of single quality flags into a flag of the general data quality

Flag of the general data quality		Steady state test according to Eq. (7.20)	Integral turbulence characteristics according to Eq. (7.21)
High quality	1	1	1–2
	2	2	1–2
	3	1–2	3–4
Reasonable	4	3–4	1–2
Quality	5	1–4	3–5
	6	5	≤5
Bad quality	7	≤6	≤6
	8	≤8	≤8
		≤8	6–8
Not to use	9		One flag equal to 9

7.2.4 Quality Control of Eddy-Covariance Data

The analysis of the data quality of the eddy-covariance method is an important issue and is one that can also be combined with the footprint technique as discussed in Sect. 8.2.3. In contrast to standard meteorological measurements, there are only a few papers available addressing quality control of eddy-covariance measurements (Foken and Wichura 1996; Vickers and Mahrt 1997). Quality control of eddy-covariance should include not only tests for instrument errors and problems with the sensors, but also evaluate how closely the conditions fulfil the theoretical assumptions underlying the method. Because the latter depends on meteorological conditions, eddy-covariance quality control tools must be a combination of a typical test for high resolution time series and an examination of the turbulent conditions. The most relevant tests are on steady-state conditions and on the fulfilment of turbulent conditions, which are given here only briefly. For details see Foken et al. (2004, 2012a).

The steady-state test used by Foken and Wichura (1996) is based on developments attributed to Russian scientists (Gurjanov et al. 1984). It compares the statistical parameters determined for the averaging period and for short intervals within this period. For instance, the time series for the determination of the covariance of the measured signals w (vertical wind) and x (horizontal wind component or scalar) of about 30 min duration will be divided into M = 6 intervals of about 5 min. N is the number of data points comprised in the short interval (N = 6,000 for 20 Hz scanning frequency and a 5 min interval):

$$\left(\overline{x'w'}\right)_i = \frac{1}{N-1}\left[\sum_j x_j \cdot w_j - \frac{1}{N}\left(\sum_j x_j \cdot \sum_j w_j\right)\right]$$
$$\overline{x'w'} = \frac{1}{M}\sum_i \left(\overline{x'w'}\right)_i \tag{7.18}$$

This value will be compared with the covariance determined for the whole interval:

$$\overline{x'w'} = \frac{1}{M \cdot N - 1}\left[\sum_{k=1}^{M \cdot N} x_k \cdot w_k - \frac{1}{M \cdot N}\left(\sum_{k=1}^{M \cdot N} x_k \cdot \sum_{k=1}^{M \cdot N} w_k\right)\right] \tag{7.19}$$

The authors proposed that the time series is steady state if the normalized difference between both covariances (parameter of relative non-stationarity)

$$RN_{Cov} = \left|\frac{\overline{(x'w')_{Eq.(7.18)}} - \overline{(x'w')_{Eq.(7.19)}}}{\overline{(x'w')_{Eq.(7.19)}}}\right| \tag{7.20}$$

is less than 30 %. This value has been found by long experience but is in good agreement with other test parameters including those of other authors (Foken and Wichura 1996). Otherwise, the data quality is likely to be lower.

The test on developed turbulent conditions based on the flux-variance similarity (Panofsky and Dutton 1984). This similarity means that the ratio of the standard deviation of a turbulent parameter and its turbulent flux is nearly constant or a function of stability. These so-called integral turbulence characteristics are basic similarity characteristics of atmospheric turbulence and are discussed in Sect. 2.2.6. These functions depend on stability and are given in Eqs. (2.62) and (2.63). The test can be done for the integral turbulence characteristics of both parameters used to determine the covariance. Similar to Eq. (7.20) both measured and the modelled parameters can be compared according to

$$ITC_\sigma = \left|\frac{\left(\sigma_x/X_*\right)_{model} - \left(\sigma_x/X_*\right)_{measurement}}{\left(\sigma_x/X_*\right)_{model}}\right| \tag{7.21}$$

If the test parameter ITC_σ is less than 30 %, a well developed turbulence can be assumed.

The quality tests given above open the possibility to also flag the quality of a single measurement (Foken and Wichura 1996; Foken et al. 2004). For these tests, the definition of flags is possible and can be combined to an overall flag (Table 7.2). The user of such a scheme must know the appropriate use of the flagged data. The presented scheme was classified by micrometeorological experience so classes 1–3 can be used for fundamental research, such as the development of parameterisations. Classes 4–6 are available for general use such as for continuously running systems of the FLUXNET programme. Classes 7 and 8 are only for orientation. It is often preferable to use such data rather than a gap filling procedure, but then these data should not differ significantly from the data located before and after these data in the time series. Data of class 9 should be excluded

Table 7.3 Eddy-covariance software tools with embedded footprint models (Foken et al. 2012a)

Software	TK3	EddySoft	EdiRE	ECO2S
	University of Bayreuth	Max-Planck-Institute Jena	University of Edinburgh	IMECC-EU University of Tuscia
Footprint tools	Kormann and Meixner (2001)	Schuepp et al. (1990)	Schuepp et al. (1990)	Kljun et al. (2004), Schuepp et al. (1990)

under all circumstances. The combination of the flagging system with the footprint analysis is given in Sect. 8.2.3.

Some of the eddy-covariance software tools include simple footprint tools for data quality control. Table 7.3 gives an overview.

7.3 Scintillometer Technique

The scintillometer (Hill et al. 1980; Hill 1997) is an optical instrument consisting of a infrared laser which measures the scintillation of the light in the atmosphere due to the movements of turbulent eddies. Essentially, scintillometers are separated into two classes (DeBruin 2002) the large aperture scintillometer (LAS) and the small aperture scintillometer (DBSAS, Fig. 7.13). The LAS has a measuring path length of several kilometres. In contrast, the DBSAS works with two laser beams over a distance of about 100 m (Andreas 1989). Temperature or humidity inhomogeneities (IR scintillometer for sensible heat flux or microwave scintillometer for latent heat flux) cause a scintillation of the measuring beam which can be evaluated. These systems can determine also the path-length-averaged turbulence scale and are also able to determine the friction velocity when a stability dependence is taken into account (Thiermann and Grassl 1992). Note that scintillometers are not able to determine the sign of the sensible heat flux. Additional measurements (temperature gradient) are necessary. In the footprint analysis, it should be stated that—in contrast with more standard measurements seeking to obtain the footprint at one location—the scintillometer-based footprint method requires that it be determined over one measuring path.

The instrument measures the refraction structure function parameter, C_n^2,

$$C_n^2 = \left(79.2 \cdot 10^{-6} \frac{p}{T^2}\right)^2 C_T^2 \tag{7.22}$$

and offers a method for the determination of the sensible heat flux $\overline{w'T'} = T_* \cdot u_*$ which is a function of the temperature structure function parameter, C_T^2 (Wyngaard et al. 1971).

Fig. 7.13 Small aperture scintillometer DBSAS, receiver unit, at Svalbard, Norway. The laser source is about 20 m away in the background (*Photograph* by Lüers, Published with kind permission of © Dr. habil. Lüers, 2012. All Rights Reserved)

$$\frac{C_T^2 \, z^{2/3}}{T_*^2} = \left\{ \begin{array}{ll} 5 \, \left(1 + 6.4 \frac{-z}{L}\right)^{-2/3} & for \; z/L \leq 0 \\ 5 \, \left(1 + 3 \frac{z}{L}\right) & for \; z/L > 0 \end{array} \right\} \tag{7.23}$$

Scintillometers have the highest sensitivity in the middle of the measurement path rather than near the transmitter and receiver. This must be taken into account for footprint analyses of the measurement sector (Meijninger et al. 2002; Göckede et al. 2005). The influence of the source area at different positions within the scintillometer path must be normalized with a weighting factor obtained by a bell-shaped weighting function (Thiermann, personal communication),

$$W(x) = A \cdot x^{11/6}(P - x)^{11/6} \tag{7.24}$$

where $W(x)$ is the weighting factor for position x in m along the measurement path with a total length P in m. A is a scaling factor that is of no importance in footprint studies.

To modify the application of footprint models for line measurements such as scintillometers, a superposition of multiple models must be implemented in software comparing land cover maps with footprints (see Chap. 6) along the measurement path. All the models must we multiplied with a path dependent factor weighting $W(x)$. The number of model runs depends on the path length and the spacing of the land cover map. In Sect. 7.4, this aggregation schema is shown for

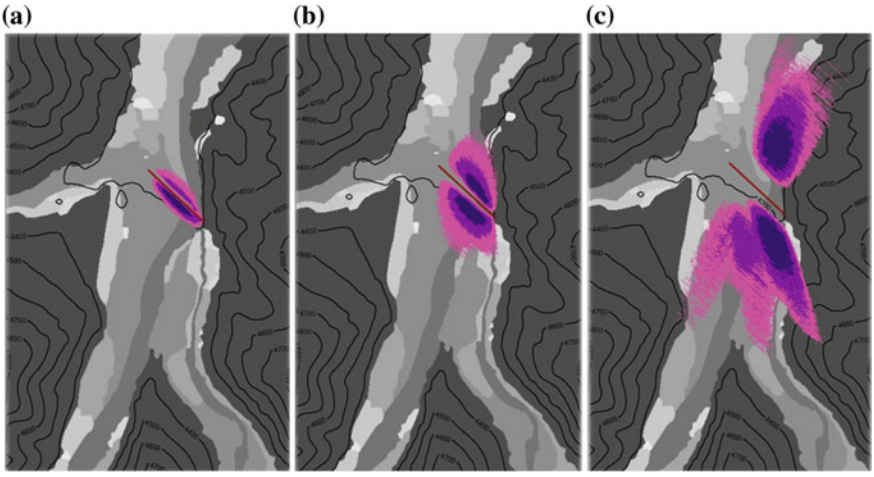

Fig. 7.14 Analysis of footprint climatology for installation of a Large Aperture Scintillometer at 20 m height on the basis of a wind climatology for unstable **a** neutral **b** and stable **c** stratification (Babel and Foken 2009, unpublished study) in a mountain valley, E-W-distance is 4 km. The contour lines are for 80, 50 and 20 % of the footprint. The different *grey areas* are different land cover classes

aircraft measurements. This schema must be modified using the weighting function according to Eq. (7.24).

In Fig. 7.14, an example of footprint climatology analysis is shown for LAS even before the installation of the instrument. The basis for this lies in the local wind climatology and the assumption of three different stability classes. It can easily be seen that only in the unstable and neutral case, the beam is over uniform terrain. Such an analysis can help to identify the optimum scintillometer location.

7.4 Airborne Measurement Technique

The first airborne study based on the data sets by Desjardins et al. (1989) was connected with the first papers pertaining to the theme of footprints (Schuepp et al. 1990). The application of airborne measurements for area-averaged turbulent fluxes becomes important in comprehensive experiments over heterogeneous landscapes like FIFE (Sellers et al. 1988), HAPEX-MOBILHY (André et al. 1990) or BOREAS (Sellers et al. 1997). Airborne fluxes showed a very heterogeneous picture and it was the first task to combine this picture with the underlying surface.

During BOREAS, the idea of application of the footprint tool became progressively evident, but first fluxes along a fly lag were compared with surface characteristics like the NDVI or tower measurements (Desjardins et al. 1997). The method to apply the footprint approach was shown and applied by Chen et al. (1999): The flux measured using airborne measurements is the sum of all fluxes of

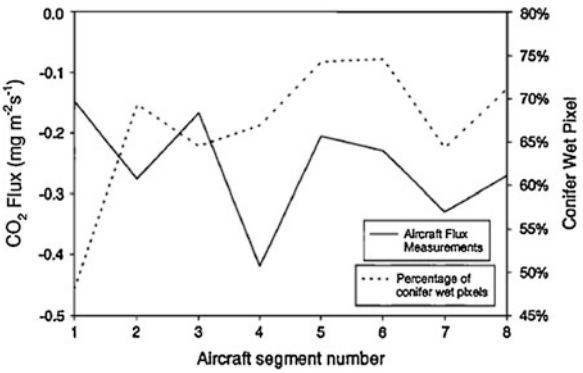

Fig. 7.15 Carbon dioxide flux measurements by an aircraft on a single line separated into eight 2 km long segments. Besides the flux the percentage of the pixels for the dominant conifer wet cover type in the footprint area is shown (Chen et al. 1999, Published with kind permission of © American Geophysical Union (Wiley), 1999. All Rights Reserved)

different flight legs—typically 2 km in most studies—and depending on a weighting function C_{kj} for each flight leg k and land use type j with M fly lags. The flux of each land use type and each flight leg is with F_j the averaged flux of each land use type:

$$F_{kj} = \sum_{k=1}^{M} C_{kj} F_j \tag{7.25}$$

The weighting function C_{kj} can be determined as

$$C_{kj} = \sum_{i=1}^{N} n_{ij} f_i \tag{7.26}$$

with i as the number of pixels in the upwind side of the flight leg and n_{ij} as the land-use type of this pixel. f_i is the footprint function which gives the weight of the pixel in the distance i. The footprint function in the case of the paper by Chen et al. (1999) was described by Kaharabata et al. (1997). An example of this first paper is given in Fig. 7.15.

This schema was too difficult to use because it was based on fluxes for each land-use type F_j measured on towers which were not representative of the whole area. Ogunjemiyo et al. (2003) proposed for the flux F_{ik} for each flight leg segment and each pixel i in this segment the following relation

$$F_{ik} = \sum_{j=1}^{K} \psi_{ijk} d_{ijk} \tag{7.27}$$

Table 7.4 Overview of key aircraft studies using footprint-related flux calculations

Airborne study	Footprint model	Remark
Desjardins et al. (1989) and Schuepp et al. (1990)	Schuepp et al. (1990)	National Aeronautical Establishment and Agriculture Canada, 1986
Schuepp et al. (1992)	Schuepp et al. (1990)	BOREAS-experiment in Canada
Chen et al. (1999)	Modification of Horst and Weil (1992, 1994) and Kaharabata et al. (1997)	BOREAS-experiment in Canada
Samuelsson and Tjernström (1999)	Schuepp et al. (1990) with modification convective conditions by Mahrt et al. (1994)	NOPEX-experiment in Sweden
Ogunjemiyo et al. (2003)	Kaharabata et al. (1997)	BOREAS-experiment in Canada, multiple regression model for aggregation
Gioli et al. (2004)	Hsieh et al. (2000)	Comparison with European FLUXNET sites
Kirby et al. (2008)	Kljun et al. (2004)	
Mauder et al. (2008)	Kljun et al. (2004) in a 2D version similar to Kormann and Meixner (2001)	GEWEX study MAGS 1999
Hutes et al. (2010)	Hsieh et al. (2000) in the 2D version by Detto et al. (2006)	Linear flux aggregation
Metzger et al. (2013)	Kljun et al. (2004) in a 2D version by Metzger et al. (2012)	China, Inner Mongolia

where d_{ijk} is the spatially averaged flux density and ψ_{ijk} a weighting function for the land cover type j. Because the flux density is difficult to measure, Ogunjemiyo et al. (2003) proposed a nonlinear multiple regression which is rarely used in most airborne data analyses. The number of pixels in the upwind direction was determined that up to 98 % of total estimated flux contribution could be included. Similar limitations comparable with the effect level approach were used by most authors. The weighting function can be determined according to

$$\psi_{ijk} = \frac{1}{R} \sum_{j}^{K} \sum_{i}^{M} I_{ijk} a_i, \tag{7.28}$$

where R is the number of pixels i in the flight segment j. $k_{ijk} = 1$ if the cover type k represents the pixel i, otherwise $I_{ijk} = 0$. a_i is a normalized footprint function for the pixel i

$$a_i = \frac{\int_{i=i_a}^{i=i_a+1} f di}{\int_{i=1}^{N} f di} \tag{7.29}$$

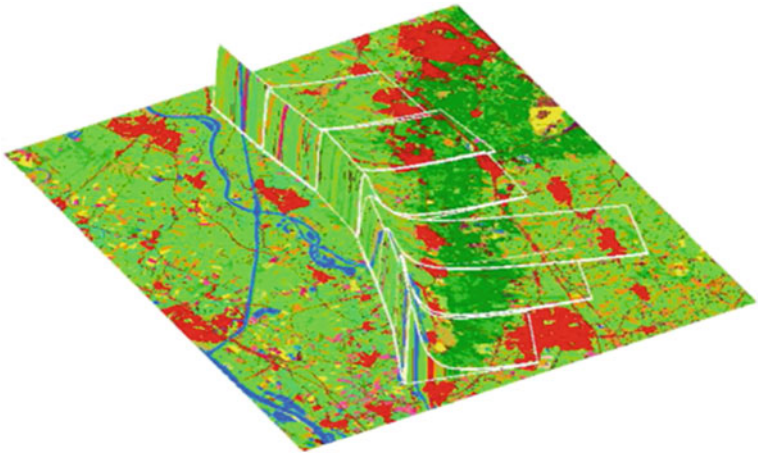

Fig. 7.16 Footprints of consecutive flux estimates along a flight track projected onto a land use map of central Netherlands. The vertical dimension gives the footprint weight, the horizontal bounds the footprint area where 90 % of the flux emanates from (Hutjes et al. 2010, Published with kind permission of © Elsevier, 2010. All Rights Reserved)

For the footprint function, Ogunjemiyo et al. (2003) used the function given by Kaharabata et al. (1997). In most aircraft studies, the above schema is applied with slight modifications (see Table 7.4). A nice example for the footprint analysis is shown by Hutjes et al. (2010) in Fig. 7.16. In contrast to earlier studies (e. g. Chen et al. 1999), the authors determine for each flight leg a footprint dependent on actual wind velocity and stability.

A deficit in aircraft footprint studies is the application of analytical approaches in homogeneous surfaces. In future studies, Lagrangian backward models or LES models should be applied. Up until now the model by Kljun et al. (2004), based on the Lagrangian backward model by Kljun et al. (2002), is used as 2D model has recognized this and included a crosswind component to their footprint models (Mauder et al. 2008; Metzger et al. 2013).

Based on aircraft investigations, Desjardins et al. (1994) pointed out that spatial variability in the flux observations can be viewed as a response to systematic changes in the flux footprint. The influence of these changes on the observed flux along a flight line can be determined from footprint investigations in combination with a linear mixing matrix. This concept has been expressed in a numerical (Chen et al. 1999) and in a regression form (Ogunjemiyo et al. 2003; Hutjes et al. 2010). Metzger et al. (2013) used these basic ideas to define an environmental response function (ERF), which relates flux observations (responses) to surface and basic meteorological properties (drivers). In their study, the land surface temperature (LST) and the enhanced vegetation index (EVI) are used as proxies for the spatial distribution of sources and sinks for sensible and latent heat, respectively. Figure 7.17 shows a low-level ($< 0.05\ z_i$) flight line of a weight-shift microlight aircraft (Metzger et al. 2011, 2012), superimposed over a land cover classification, LST and EVI from MODIS,

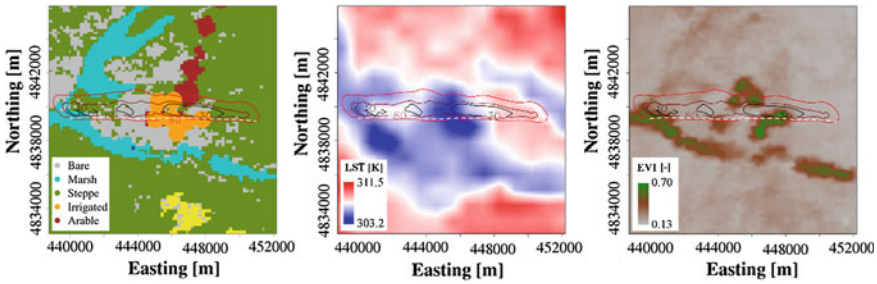

Fig. 7.17 Flight along a pattern over Northeast China on 8 July 2009, 12:16–12:24 BST (*white dashed line*) from (Metzger et al. 2013). The composite flux footprint along the flight line (30, 60, 90 % *contour lines*) is superimposed over maps of land cover (*left panel*), land surface temperature (LST, *center panel*), and enhanced vegetation index (EVI, *right panel*) Published with kind permission of © Copernicus Publications, distributed under the Creative Commons Attribution 3.0 License, 2007. All Rights Reserved

respectively. Generally speaking, the medium spatial resolution (250–1000 m) of the MODIS data is less-than-ideal, but more importantly, the MODIS satellite data enables considering temporal changes in the surface properties. In contrast to prior attempts, Metzger et al. (2013) used (i) time-frequency analysis to increase the sample size along a flight line (ii) continuous and contemporary representations of the land cover, and (iii) a non-parametric machine learning technique (Elith et al. 2008) to determine the ERFs. The resulting parameter of determination between the drivers and the fluxes of sensible and latent heat was surprisingly high with $R^2 \approx 0.99$. Provided the ERFs are well calibrated using direct flux measurements, this method can be used to determine spatially resolved turbulent fluxes remote sensing data to within 20 % accuracy.

References

Akima H (1970) A new method of interpolation and smooth curve fitting based on local procedures. J Assc Comp Mach 17:589–602

André J-C, Bougeault P, Goutorbe J-P (1990) Regional estimates of heat and evaporation fluxes over non-homogeneous terrain, examples from the HAPEX-MOBILHY programme. Bound-Layer Meteorol 50:77–108

Andreas EL (1989) Two-wavelength method of measuring path-averaged turbulent surface heat fluxes. J Atm Oceanic Tech 6:280–292

Arya SP (2001) Introduction to micrometeorology. Academic Press, San Diego 415 pp

Aubinet M (2008) Eddy covariance CO_2 flux measurements in nocturnal conditions: an analysis of the problem. Ecol Appl 18:1368–1378

Aubinet M, Vesala T, Papale D (2012) Eddy covariance: a practical guide to measurement and data analysis. Springer, Dordrecht 438 pp

Baldocchi D (1997) Flux footprints within and over forest canopies. Bound-Layer Meteorol 85:273–292

Bowen IS (1926) The ratio of heat losses by conduction and by evaporation from any water surface. Phys Rev 27:779–787

Businger JA (1982) Equations and concepts. In: Nieuwstadt FTM, Van Dop H (eds) Atmospheric turbulence and air pollution modelling: a course held in the hague, 21-25 September 1981. D. Reidel Publishing Company, Dordrecht, pp 1–36

Businger JA (1986) Evaluation of the accuracy with which dry deposition can be measured with current micrometeorological techniques. J Appl Meteorol 25:1100–1124

Chen JM, Leblanc SG, Cihlar J, Desjardins RL, MacPherson IJ (1999) Extending aircraft- and tower-based CO_2 flux measurements to a boreal region using a Landsat thematic mapper land cover map. J Geophys Res 104(D14):16,859–816,877

DeBruin HAR (2002) Introduction: renaissance of scintillometry. Bound-Layer Meteorol 105:1–4

Desjardins RL, MacPherson JI, Schuepp PH, Karanja F (1989) An evaluation of aircraft flux measurements of CO_2, water vapor and sensible heat. Bound-Layer Meteorol 47:55–69

Desjardins RL, MacPherson JI, Schuepp PH, Hayhoe HN (1994) Airborne flux measurements of CO_2, sensible, and latent heat over the hudson bay lowland. J Geophys Res Atmos 99:1551–1561

Desjardins RL et al (1997) Scaling up flux measurements for the boreal forest using aircraft-tower combination. J Geophys Res 102(D24):29125–29133

Detto M, Montaldo N, Albertson JD, Mancini M, Katul G (2006) Soil moisture and vegetation controls on evapotranspiration in a heterogeneous mediterranean ecosystem on sardinia. Italy Water Resour Res 42:W08419

Dugas WA, Fritschen LJ, Gay LW, Held AA, Matthias AD, Reicosky DC, Steduto P, Steiner JL (1991) Bowen ratio, eddy correlation, and portable chamber measurements of sensible and latent heat flux over irrigated spring wheat. Agric For Meteorol 56:12–20

Elith J, Leathwick JR, Hastie T (2008) A working guide to boosted regression trees. J Anim Ecol 77:802–813

Finnigan JJ, Clement R, Malhi Y, Leuning R, Cleugh HA (2003) A re-evaluation of long-term flux measurement techniques, part I: averaging and coordinate rotation. Bound-Layer Meteorol 107:1–48

Foken T, Wichura B (1996) Tools for quality assessment of surface-based flux measurements. Agric For Meteorol 78:83–105

Foken T, Richter SH, Müller H (1997) Zur Genauigkeit der Bowen-Ratio-Methode. Wetter Leben 49:57–77

Foken T (1998) Genauigkeit meteorologischer Messungen zur Bestimmung des Energie- und Stoffaustausches über hohen Pflanzenbeständen. Ann Meteorol 37:513–514

Foken T, Göckede M, Mauder M, Mahrt L, Amiro BD, Munger JW (2004) Post-field data quality control. In: Lee X et al (eds) Handbook of micrometeorology: a guide for surface flux measurement and analysis. Kluwer, Dordrecht, pp 181–208

Foken T (2008) Micrometeorology. Springer, Berlin, 308 pp

Foken T, Leuning R, Oncley SP, Mauder M, Aubinet M (2012a) Corrections and data quality. In: Aubinet M et al (eds) Eddy covariance: a practical guide to measurement and data analysis. Springer, Dordrecht, pp 85–131

Foken T, Aubinet M, Leuning R (2012b) The eddy-covarianced method. In: Aubinet M et al (eds) Eddy covariance: a practical guide to measurement and data analysis. Springer, Dordrecht, pp 1–19

Fritschen LJ, Fritschen CL (2005) Bowen ratio energy balance method. In: Hatfield JL, Baker JM (eds) Micrometeorology in agricultural systems. American Society of Agronomy, Madison, pp 397–405

Gioli B et al (2004) Comparison between tower and aircraft-based eddy covariance fluxes in five European regions. Agric For Meteorol 127:1–16

Göckede M, Markkaken T, Mauder M, Arnold K, Leps JP, Foken T (2005) Validation of footprint models using natural tracer measurements from a field experiment. Agric For Meteorol 135:314–325

Gurjanov AE, Zubkovskij SL, Fedorov MM (1984) Mnogokanalnaja avtomatizirovannaja sistema obrabotki signalov na baze EVM (automatic multi-channel system for signal analysis with electronic data processing). Geod Geophys Veröff R II 26:17–20

Haugen DA (ed) (1973) Workshop on micrometeorology. American Meteorological Society, Boston, 392 pp
Hill R (1997) Algorithms for obtaining atmospheric surface-layer from scintillation measurements. J Atm Oceanic Tech 14:456–467
Hill RJ, Clifford SF, Lawrence RS (1980) Refractive index and absorption fluctuations in the infrared caused by temperature, humidity and pressure fluctuations. J Opt Soc Am 70:1192–1205
Horst TW, Weil JC (1992) Footprint estimation for scalar flux measurements in the atmospheric surface layer. Bound-Layer Meteorol 59:279–296
Horst TW, Weil JC (1994) How far is far enough?: the fetch requirements for micrometeorological measurement of surface fluxes. J Atm Oceanic Tech 11:1018–1025
Horst TW (1999) The footprint for estimation of atmosphere-surface exchange fluxes by profile techniques. Bound-Layer Meteorol 90:171–188
Hsieh C-I, Katul G, Chi T-W (2000) An approximate analytical model for footprint estimation of scalar fluxes in thermally stratified atmospheric flows. Adv Water Res 23:765–772
Hutjes RWA, Vellinga OS, Gioli B, Miglietta F (2010) Dis-aggregation of airborne flux measurements using footprint analysis. Agric For Meteorol 150:966–983
Kaharabata SK, Schuepp PH, Ogunjemiyo S, Shen S, Leclerc MY, Desjardins RL, MacPherson JI (1997) Footprint considerations in BOREAS. J Geophys Res 102(D24):29113–29124
Kaimal JC, Finnigan JJ (1994) Atmospheric boundary layer flows: their structure and measurement. Oxford University Press, New York 289 pp
Kirby S, Dobosy R, Williamson D, Dumas E (2008) An aircraft-based data analysis method for discerning individual fluxes in a heterogeneous agricultural landscape. Agric For Meteorol 148:481–489
Kljun N, Rotach MW, Schmid HP (2002) A three-dimensional backward Lagrangian footprint model for a wide range of boundary layer stratification. Bound-Layer Meteorol 103:205–226
Kljun N, Calanca P, Rotach M, Schmid HP (2004) A simple parameterization for flux footprint predictions. Bound-Layer Meteorol 112:503–523
Kormann R, Meixner FX (2001) An analytical footprint model for non-neutral stratification. Bound-Layer Meteorol 99:207–224
Leclerc MY, Thurtell GW (1990) Footprint prediction of scalar fluxes using a Markovian analysis. Bound-Layer Meteorol 52:247–258
Lee X (2004) A model for scalar advection inside canopies and application to footprint investigation. Agric For Meteorol 127:131–141
Lee X, Massman WJ, Law B (eds) (2004) Handbook of micrometeorology: a guide for surface flux measurement and analysis. Kluwer, Dordrecht, 250 pp
Liu H, Foken T (2001) A modified Bowen ratio method to determine sensible and latent heat fluxes. Meteorol Z 10:71–80
Mahrt L, Sun J, Vickers D, MacPherson JI, Pederson JR, Desjardins RL (1994) Observations of fluxes and inland breezes over a heterogeneous surface. J Atmos Sci 51:2484–2499
Marquardt D (1983) An algorithm for least-squares estimation of nonlinear parameters. J Soc Ind Appl Math 11:431–441
Mauder M, Desjardins R, MacPherson I (2008) Creating surface flux maps from airborne measurements: application to the Mackenzie area GEWEX study MAGS 1999. Bound-Layer Meteorol 129:431–450
Meijninger WML, Green AE, Hartogensis OK, Kohsiek W, Hoedjes JCB, Zuurbier RM, DeBruin HAR (2002) Determination of area-averaged water vapour fluxes with large aperture and radio wave scintillometers over a heterogeneous surface: Flevoland field experiment. Bound-Layer Meteorol 105:63–83
Metzger S, Junkermann W, Butterbach-Bahl K, Schmid HP, Foken T (2011) Corrigendum to "Measuring the 3-D wind vector with a weight-shiftmicrolight aircraft" published in atmospheric measuring technique, 4:1421–1444, 1515–1539

Metzger S, Junkermann W, Mauder M, Beyrich F, Butterbach-Bahl K, Schmid HP, Foken T (2012) Eddy-covariance flux measurements with a weight-shift microlight aircraft. Atmos Meas Tech 5:1699–1717

Metzger S et al (2013) Spatial resolution and regionalization of airborne flux measurements using environmental response functions. Biogeochemistry 10:2193–2217

Moncrieff J (2004) Surface turbulent fluxes. In: Kabat P et al (eds) Vegetation, water, humans and the climate: a new perspective on an interactive system. Springer, Berlin, pp 173–182

Nappo CJ et al (1982) The workshop on the representativeness of meteorological observations, June 1981, Boulder CO. Bull Am Meteorol Soc 63:761–764

Nieuwstadt FTM (1978) The computation of the friction velocity u_* and the temperature scale T_* from temperature and wind velocity profiles by least-square method. Bound-Layer Meteorol 14:235–246

Ogunjemiyo SO, Kaharabata SK, Schuepp PH, MacPherson IJ, Desjardins RL, Roberts DA (2003) Methods of estimating CO_2, latent heat and sensible heat fluxes from estimates of land cover fractions in the flux footprint. Agric For Meteorol 117:125–144

Ohmura A (1982) Objective criteria for rejecting data for Bowen ratio flux calculations. J Climate Appl Meteorol 21:595–598

Panofsky HA, Dutton JA (1984) Atmospheric turbulence: models and methods for engineering applications. Wiley, New York 397 pp

Rannik Ü, Aubinet M, Kurbanmuradov O, Sabelfeld KK, Markkanen T, Vesala T (2000) Footprint analysis for measurements over heterogeneous forest. Bound-Layer Meteorol 97:137–166

Rannik Ü, Markkanen T, Raittila T, Hari P, Vesala T (2003) Turbulence statistics inside and above forest: Influence on footprint prediction. Bound-Layer Meteorol 109:163–189

Samuelsson P, Tjernström M (1999) Airborne flux measurements in NOPEX: comparison with footprint estimated surface heat fluxes. Agric For Meteorol 98–99:205–225

Schmid HP (1997) Experimental design for flux measurements: matching scales of observations and fluxes. Agric For Meteorol 87:179–200

Schotanus P, Nieuwstadt FTM, DeBruin HAR (1983) Temperature measurement with a sonic anemometer and its application to heat and moisture fluctuations. Bound-Layer Meteorol 26:81–93

Schuepp PH, Leclerc MY, MacPherson JI, Desjardins RL (1990) Footprint prediction of scalar fluxes from analytical solutions of the diffusion equation. Bound-Layer Meteorol 50:355–373

Schuepp PH, MacPherson JI, Desjardins RL (1992) Adjustment of footprint correction for airborne flux mapping over the FIFE site. J Geophys Res 97(D17):18455–18466

Sellers PJ, Hall FG, Asrar G, Strebel DE, Murphy RE (1988) The first ISLSCP field experiment (FIFE). Bull Am Meteorol Soc 69:22–27

Sellers PJ et al (1997) BOREAS in 1997: experiment overview, scientific results, and future directions. J Geophys Res 102:28(769)731–728

Stannard DI (1997) A theoretically based determination of Bowen-ratio fetch requirements. Bound-Layer Meteorol 83:375–406

Stull RB (1988) An introduction to boundary layer meteorology. Kluwer Academic Publisher, Dordrecht, 666 pp

Tanner BD (1988) Use requirements for Bowen ratio and eddy correlation determination of evapotranspiration. In: Proceedings of the 1988 speciality conference of the irrigation and drainage devisions, ASCE Lincoln, Nebraska, 19–21 July 1988

Thiermann V, Grassl H (1992) The measurement of turbulent surface layer fluxes by use of bichromatic scintillation. Bound-Layer Meteorol 58:367–391

Vickers D, Mahrt L (1997) Quality control and flux sampling problems for tower and aircraft data. J Atm Oceanic Tech 14:512–526

Wilczak JM, Oncley SP, Stage SA (2001) Sonic anemometer tilt correction algorithms. Bound-Layer Meteorol 99:127–150

Wyngaard JC, Izumi Y, Collins SA (1971) Behavior of the refractive-index-structure parameter near the ground. J Opt Soc Am 61:1646–1650